Dalton Transactions

Accepted Manuscript

This is an *Accepted Manuscript*, which has been through the Royal Society of Chemistry peer review process and has been accepted for publication.

Accepted Manuscripts are published online shortly after acceptance, before technical editing, formatting and proof reading. Using this free service, authors can make their results available to the community, in citable form, before we publish the edited article. We will replace this *Accepted Manuscript* with the edited and formatted *Advance Article* as soon as it is available.

You can find more information about *Accepted Manuscripts* in the Information for Authors.

Please note that technical editing may introduce minor changes to the text and/or graphics, which may alter content. The journal's standard Terms & Conditions and the Ethical guidelines still apply. In no event shall the Royal Society of Chemistry be held responsible for any errors or omissions in this *Accepted Manuscript* or any consequences arising from the use of any information it contains.

ROYAL SOCIETY OF CHEMISTRY

www.rsc.org/dalton

Cite this: DOI: 10.1039/c0xx00000x

www.rsc.org/xxxxxx

ARTICLE TYPE

Reduced graphene oxide/$Ni_{1-x}Co_xAl$-layered double hydroxide composites: preparation and high supercapacitor performance

Jie Xu,[a] Shili Gai,[a] Fei He,[a] Na Niu,[a] Peng Gao,*[a] Yujin Chen*[b] and Piaoping Yang*[a]

Received (in XXX, XXX) Xth XXXXXXXXX 20XX, Accepted Xth XXXXXXXXX 20XX

DOI: 10.1039/b000000x

Reduced graphene oxide sheets (rGO) and ternary-component $Ni_{1-x}Co_xAl$-layered double hydroxide ($Ni_{1-x}Co_xAl$-LDH) hybrid composites with interesting sandwich structure have been fabricated by an *in situ* growth route. The as-obtained composite displays a sandwich architecture constructed by the self-assembly of sheet-like LDH crystals on both sides of rGO sheets. It was found that the Co content doped in $Ni_{1-x}Co_xAl$-LDH plays an important role in the shape and structure of the final products. When the Co doped content is 17%, the rGO/$Ni_{0.83}Co_{0.17}Al$-LDH preserves high surface area (171.5 m^2/g) and exhibits a perfect sandwich structure. In addition, this structure and morphology would be favorable as supercapacitor electrode material for high performance. Influence of cobalt content on the electrochemical behaviors of rGO/$Ni_{1-x}Co_xAl$-LDH has been systematically studied. The results indicate that rGO/$Ni_{0.83}Co_{0.17}Al$-LDH composite exhibits highest electrochemical performance: the specific capacitance of 1902 F/g at 1 A/g and excellent cycling stability. The markedly improved electrochemical performance superior to undoped rGO/NiAl-LDH should be attributed to the enhanced conductivity through cobalt doping. This kind of composites should be a kind of potential energy storage/conversion material for supercapacitor.

1. Introduction

Nowadays, supercapacitors have gained much attention owing to their outstanding superiorities compared to conventional dielectric capacitors and secondary batteries, including fast charging/discharging rate, high power density and long cycle life.[1–4] Another important reason for the motivated development of supercapacitors is the aggravating environment and resource issues from the non-renewable fossil fuels.

Generally, there are two types of supercapacitors in terms of their charge storage mechanisms. One is the electrical double layer capacitors (EDLCs), which is based on the electrostatic process. Thus the electrode materials with good conductivity and large specific surface areas are beneficial to the energy storage process of EDLCs. Among them, carbon-based materials including activated carbon, CNTs, carbon nanofibers, and the emerging graphene-based 2D sheets are undisputed to be excellent electrode materials for EDLCs.[5–8] The most worthy of mention is graphene-based materials, especially reduced graphene oxide (rGO) due to their chemically active surface with large specific area, good conductivity, low cost, and mass production with solution-based process ability.[2,5,9,10] Moreover, the aggregated graphene sheets exhibit an open-pore structure allowing for the easy access of electrolyte ions to form electric double layers.[11] Pseudocapacitor is the other type of supercapacitor based on the fast redox reactions. The common electrode materials for pseudocapacitor usually include conducting polymers (polyaniline, polypyrrole),[12–14] transition metal (Ru, Co, Ni, Mn, etc.) oxides[15–18] and hydroxides.[19–21] Pseudocapacitor can afford higher specific capacitance and faster redox kinetics compared to carbon based EDLCs electrode.[11,22] However, the used metal oxides especially RuO_2 have a relatively high price,[23] and the conducting polymers usually possess the low conductivity. Both of the reasons have limited their applications. Those issues can be mitigated by combining carbon based materials with metal oxides/conducting polymers to compose the hybrid type of supercapacitor (in other words, the combination of the EDLCs and pseudo-capacitor). Compared with traditional carbon-based electrode materials, graphene is a monolayer of carbon atoms arranged in a honeycomb network with high conductivity, superior electron mobility and extremely high specific surface area, which is an ideal substrate to grow, anchor and assemble nanomaterials for excellent functional materials. Thus graphene based composites, such as rGO/Co_3O_4,[16] graphene/NiO,[17] rGO/MnO_2,[18,22] graphene/NiAl-LDHs,[24] have stimulated exploding interests in supercapacitor field.

Layered double hydroxides (LDHs) containing transition metals have been extensively employed as supercapacitor electrode materials due to their low cost, high redox activity, and environmentally friendly nature.[19,24–26] Furthermore, LDHs discribed as a generic formula $[M^{2+}_{1-x}M^{3+}_x(OH)_2]^{x+}[A^{n-}]_{x/n}.mH_2O$ (M^{2+} and M^{3+} are the respective divalent and trivalent metal cations; A^{n-} is a interlayer anion), are promising inorganic materials in view of their tunable composition, the ability of anion exchange and capacity to intercalate anions.[27] They are

Dalton Transactions Accepted Manuscript

widely used in the fields of catalysis,[28,29] anion exchange,[30] optoelectronic functional materials,[24,31–33] absorbent[34,35] and biology.[26,36–39] Recently, much attention has been paid on the reaseach of LDHs for electrochemical performance, including NiAl-LDH[33], CoAl-LDH,[40,41] NiCoAl-LDH[42] and their carbon-based composites.[8,43,44] As for $Ni_{1-x}Co_xAl$-LDH, partial nickel sites are substituted by Co. By doping a certain amount of Co^{2+} ions, the ternaty-component NiCoAl-LDH exhibits higher electrochemical performance in comparison to any binary-component NiAl-LDH or CoAl-LDH.[8] It is ascribed to the increased electrochemical active sites derived from the incorporation of another transition metal cation and the enhanced conductivity owing to the existance of Co element.[45] Therein the increase of electronic conductivity from the substitution of cobalt into NiAl-LDH, because the effect of d-electrons of Ni(II) and CoOOH can serve as a good current collector.[46] Gupta *et al*. found that nanostructured $Co_{0.59}Ni_{0.21}Al_{0.20}$-LDHs had a maximum specific capacitance of 1263F g^{-1}.[42] Yang *et al*. reported that the specific capacitance of NiCoAl-LDH and carbon nanotube nanohybrid reached 1035 F/g at a current density of 1 A/g.[8] Howerver, the ternary-component NiCoAl-LDH and graphene nanohybrids for pseudocapacitor electrode materials have rarely been reported. Furthermore, the synthetic route induced conventional structure and shape of the as-reported materials determine the relatively low electrochemical performance. Thus, developing a novel method to fabricate ternary-component LDH/rGO hybrid composite with interesting structure favorable for elecrode materials should be highly promising.

Herein, we prepared a series of NiCoAl-LDH/rGO nanohybrids with various Co doped contents by an *in situ* growth process. After AlOOH colloids were coated on both sides of rGO, LDH graphene hybrid composites with interesting sandwich structure were prepared using graphene oxide sheets as building block. By doping different contents of Co, the as-obtained $rGO/Ni_{1-x}Co_xAl$-LDH composites with a morphology evolution were used as electrode materials to examine the electrochemical performance in comparition with rGO/NiAl-LDH. Moreover, preliminary studies about the effect of $rGO/Ni_{1-x}Co_xAl$-LDH composition on their capacitive properties have also been investigated. Owing to the favourable morphology, large specific surface area (171.5 m^2/g) and enhanced conductivity, the $Ni_{0.83}Co_{0.17}Al$-LDH graphene composite exhibited the highest specific capacitance of 1902 F/g at a current density of 1 A/g. The specific capacitance of $rGO/Ni_{0.83}Co_{0.17}Al$-LDH only decreases from 1415 to 873 F/g after 1500 cycles, and more than 63% of the initial capacitance can be retained at the high current density of 10 A/g. The excellent peformance behavior and good cycling stability at high rates make it a promising electrode material for supercapacitors.

2. Experimental section

2.1. Synthesis of $rGO/Ni_{1-x}Co_xAl$-LDH

Firstly, the graphene oxide (GO) nanosheets used in this study were prepared by Hummers method with some modification.[9] Typically, 1.0 g of graphite powder was mixed with 23 mL H_2SO_4 under vigorous stirring for 1 h in an ice bath. Then, 6.0 g of $KMnO_4$ was slowly added into the mixture and the temperature of the system was kept below 5 °C in an ice bath under another vigorous stirring for 3 h. Subsequently, the reaction mixture was heated to 40 °C and maintained at 40 °C for 1 h until it became pasty brownish, then 80 mL of deionized water was slowly added, After stirring for 15 min, 60 mL of deionized water was added into the mixture. A solution containing 10 mL of 30 wt% H_2O_2 and 60 mL of deionized water was added to the mixture to reduce the residual $KMnO_4$, after which the color of the mixture turned in golden yellow, followed by repeated washings with deionized water to remove the acids and metal ions. Then the aqueous suspension of GO (1 g L^{-1}) was obtained by dissolving GO in deionized water with an ultrasonic bath (KQ-600KDE, 600 W). After preparing AlOOH from the hydrolysis process of aluminum isopropoxide,[47] the GO@AlOOH was prepared by a layer-by-layer (LBL) method. The growth of $Ni_{1-x}Co_xAl$-LDH on the graphene nanosheets was through an *in situ* crystallization process.[48] Briefly, 6 mL GO solution was put into 20 mL AlOOH sol by aging for 12 h. The GO@AlOOH was separated by centrifugation, rinsed with ethanol and dried at room temperature. Then the GO@AlOOH was redispersed in 30 mL deionized water. Subsequently, 0.6 g urea and stoichiometric $Ni(NO_3)_2$ and $Co(NO_3)_2$ was added into above solution for a hydrothermal treatment at 100 °C for 24 h. The molar content of $Ni(NO_3)_2$ and $Co(NO_3)_2$ was kept to be 1.5 mmol in the reaction. Then the Ni^{2+}/Co^{2+} molar ratio of 5:1, 2:1, 1:1, 1:2 and 1:5 was altered during the synthesis procedure. The as-obtained $rGO/Ni_{1-x}Co_xAl$-LDH composites after hydrothermal reaction was collected by centrifugation, washed with deionized water and ethanol for several times. Finally, the samples were dried at 60 °C for the following characterization and electrochemical tests. The composites prepared with the Ni^{2+}/Co^{2+} molar ratio of 5:1, 2:1, 1:1, 1:2 and 1:5 were designated as RGL1, RGL2, RGL3, RGL4 and RGL5, respectively.

2.2. Characterization

The crystalline structure and detailed shapes of the products were analyzed by X-ray diffraction (XRD, Rigaku D/max-TTR-III) using Cu Kα radiation (λ = 0.15405 nm), scanning electron microscope (SEM, JSM-6480A, Japan Electronics) with an energy dispersive X-ray spectrometry analyzer (EDS, INC250, Japan Electronic), Transmission electron microscopy (TEM) and high-resolution transmission electron microscopy (HRTEM) (FEI Tecnai G^2 S-Twin) with a field emission gun operating at 200 kV. Inductively coupled plasma (ICP) measurements were taken on Thermo iCAP 6000 ICPOES. Raman spectra were taken on a Renishaw RM2000 Raman spectrometer with 457.9 nm wavelength incident laser light. The X-ray photoelectron spectra (XPS) were recording on a VG ESCALAB MK II electron energy spectrometer using Mg KR (1253.6 eV) as the X-ray excitation source. N_2 adsorption/desorption were measured by the Brunauer-Emmett-Teller (BET) using a Micromeritics TriStar II 3020 instrument. All the measurements were performed at room temperature.

2.3. Preparation of electrodes and electrochemical characterization

The electrochemical properties of as-prepared products were investigated by using a conventional three-electrode cell with a

Dalton Transactions Accepted Manuscript

This journal is © The Royal Society of Chemistry [year]

saturated calomel electrode (SCE) as the reference electrode, Pt foil as the counter electrode, Ni foam coated with active material as working electrode, and 6 mol/L KOH aqueous solution as the electrolyte. The working electrodes were prepared by mixing the as-obtained composites, acetylene black and polytetrafluoro ethylene (PTFE) at a weight ratio of 80: 15: 5 to obtain a homogeneous slurry with addition of a small amount of ethanol, which were pasted on the nickel foam substrate and dried at 60 °C for 8 h in a vacuum oven. A CHI660D electrochemical workstation was employed for cyclic voltammograms, galvanostatic charge/discharge curves, and electrochemical impedance spectroscopy (EIS). The specific capacitance (C_{sp}) was calculated from the equation $C_{sp} = \Delta t\ I/\Delta V\ m$, where Δt is the discharging time (s), I is the constant discharge current (A), ΔV is the voltage drop upon discharging (V), and m is the mass of as-obtained graphene composites in the electrode (g), respectively.

3. Result and discussion

3.1. Phase, structure and morphologies of rGO/$Ni_{1-x}Co_xAl$-LDH

First of all, the as-obtained rGO/$Ni_{1-x}Co_xAl$-LDH composites prepared from the *in situ* growth process were measured by EDS to get the atomic percentages (atom%) of the Co, Ni, Al and C elements in the samples (Fig. S1). And the results are list in Table S1. As shown, the Ni^{2+}/Co^{2+} molar ratio is basically proportional to that in the initial solution. The composites are denoted as rGO/$Ni_{0.83}Co_{0.17}$CAl-LDH (RGL1), rGO/$Ni_{0.67}Co_{0.33}$Al-LDH (RGL2), rGO/$Ni_{0.50}Co_{0.50}$Al-LDH (RGL3), rGO/$Ni_{0.33}Co_{0.67}$Al-LDH (RGL4), rGO/$Ni_{0.17}Co_{0.83}$Al-LDH (RGL5) and rGO/CoAl-LDH with the increased molar content of $Co(NO_3)_2$. Furthermore, as shown in the Table S2, ICP measurements show the similar results to the EDS analyses, indicating that as-resulting five rGO/NiCoAl-LDH composites have the element compositions and Ni/Co molar ratios as desired. Therein the (Ni + Co)/Al molar ratio is about 3 in the graphene composites.

Fig. 1 shows the XRD patterns of GO, rGO and RGL1, respectively. It is found that the as-prepared GO displays a layered structure with an interlayer spacing of 0.86 nm corresponding to the feature diffraction peak at 10.2°, revealing the introduction of oxygen functional groups on the graphite sheets.[45,48] For rGO, an obvious peak representing an interlayer spacing of 0.37 nm is found, which can be ascribed to the reduction of GO and the disordered stacking of rGO.[31] From the XRD pattern of as-prepared rGO/$Ni_{0.83}Co_{0.17}$Al-LDH hybrid composite, we can see a series of (003), (006), (012), (015), (018), (110), (113) and (116) reflections indexed to a typical hydrotalcite-like structure (JCPDS No. 15-0087), indicating the phase transformation from the AlOOH colloids to LDH.[33,43,47] It is noted that no peaks related with rGO appears in the pattern. Recent reports reveal that, if the regular stacks of graphene oxide are destroyed by exfoliation, their diffraction peaks would become weak or even disappear.[18,49] Thus, the LDH in the composite may prevent the restacking of graphene nanosheets, resulting in the broken of the regular lamellar structure of GO sheets, which is further proved by the following Raman results. Fig. S2 gives the XRD patterns of rGO/$Ni_{1-x}Co_xAl$-LDH composites with different Ni/Co molar ratios. It is obvious that all rGO/$Ni_{1-x}Co_xAl$-LDH shows much similar peaks at 11.8°, 23.5°, 34.6°, 39.2°, 60.2° and 61.6° indexed directly to the hydrotalcite-like $Ni_6Al_2CO_3(OH)_{16}{\cdot}4H_2O$ compound.

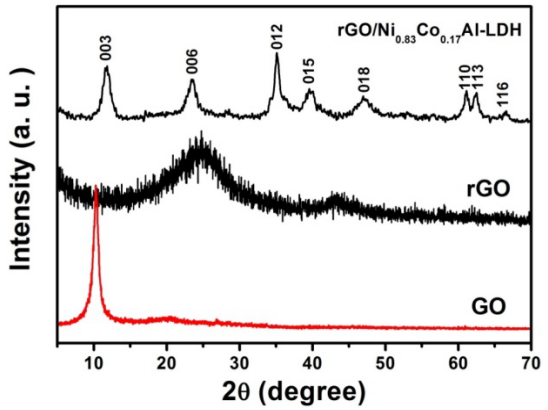

Fig. 1 XRD patterns of GO, rGO, and rGO/$Ni_{0.83}Co_{0.17}$Al-LDH.

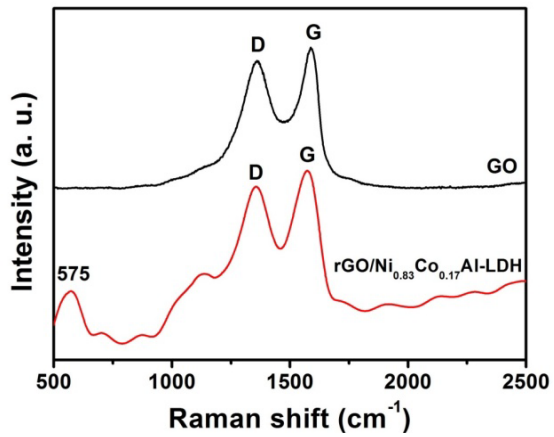

Fig. 2 Raman spectra of rGO/$Ni_{0.83}Co_{0.17}$Al-LDH and GO.

The lattice vibration and chemical bonding character of the as-obtained samples were studied by Raman spectroscopy. As shown in Fig. 2, the main features in the Raman spectra of rGO/LDH and GO are D and G bands centered at around 1350 and 1585 cm^{-1}. Wherein, the respective D and G peak corresponds to the K-point phonons of A_{1g} symmetry and zone center phonons of E_{2g} symmetry.[10,50] As the D phonon mode is optically active only in the presence of disorder, it provides a measure of the disorder of carbon species.[44,51] It can be seen that the intensity ratio of the D/G peaks decreases in rGO/LDH in comparison with that in GO, indicating the decrease in the size of the in-plane sp^2 domains due to the removal of the oxygen containing groups in the composite after the hydrothermal process.[48,50,52] It is in good accordance with the XRD results (Fig. 1). Another obvious peak centered at 575 cm^{-1} in rGO/LDH is typically assigned to LDH,[53] indicating the existence of LDH in the composite. The XPS spectra of as-obtained rGO/LDH are presented in Fig. S3. In the C 1s spectrum of rGO/LDH (Fig. S3B), deconvolution of the core-level C1s spectrum gives five types of carbon bonds: sp2 C (284.6 eV), sp3 C (285.6 eV), C-O (286.5 eV), C=O (287.8 eV) and O-C=O (288.5 eV).[51] According to the work,[48] the percentages of the peak areas of sp2 C and sp3 C bonds are dominated in the C1s spectrum, indicating the

Dalton Transactions Accepted Manuscript

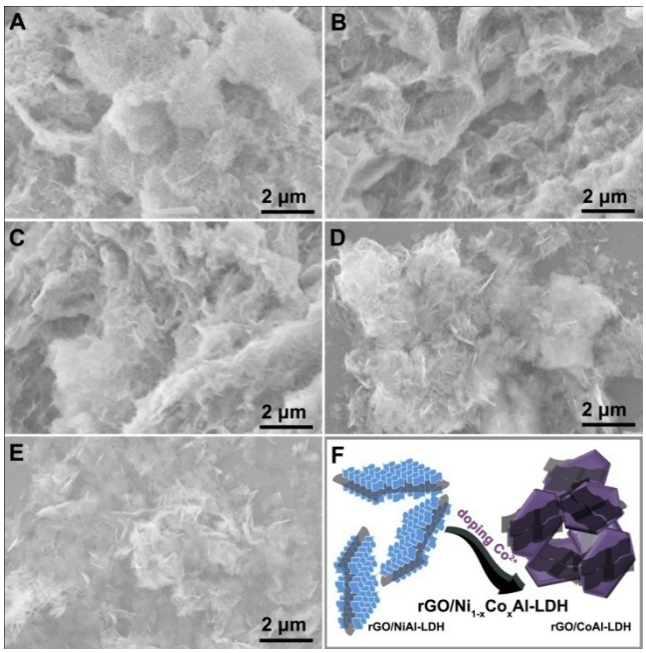

Fig. 3 SEM images of rGO/$Ni_{1-x}Co_xAl$-LDH with x values of (A) 0.17, (B) 0.33, (C) 0.5, (D) 0.67, (E) 0.83, and (F) schematic illustration for the shape conversion from rGO/NiAl-LDH to rGO/CoAl-LDH composite.

removal of oxygen containing groups in the composite, which well matches with the XRD and Raman results. Furthermore, the Ni 2p and Co 2p spectra (Fig. S3C and D) confirm the existence of Ni^{2+} and Co^{2+} in the Co-doped LDH graphene composites.[8]

The morphology evolution of the rGO/$Ni_{1-x}Co_xAl$-LDH composites with different Co doping was studied by the SEM images (Fig. 3). In Fig. 3A for RGL1 (17mol% Co), the typical hexagonal lamellar LDH sheets grow orderly on graphene substrate, displaying an interesting sandwich structure. No obvious changes can be found when the cobalt content was increased to 33 mol% (RGL2) and 50 mol% (RGL3), as shown in Fig. 3B and C. From Fig. 3D and E for RGL4 (67 mol%) and RGL5 (83 mol%), we can see that the LDH nanosheets with much larger particle size irregularly grow/attach on the graphene substrate. Thus it is inferred that the Co composition plays an important role in the morphology evolution. Fig. 3F schematically represents the shape evolution from rGO/NiAl-LDH to rGO/CoAl-LDH composite. The detailed morphology and structure of the composite were further investigated by means of SEM and TEM, as given in Fig. 4. For the as-prepared GO (Fig. 4A), the product shows the characteristic thin and curled nanosheet structure. In Fig. 4B for pure $Ni_{0.83}Co_{0.17}Al$-LDH, the sample consists of numerous nanosheets which disperse disorderly. From the SEM image of rGO/$Ni_{0.83}Co_{0.17}Al$-LDH (Fig. 4C), we can see that the shape and structure of rGO/$Ni_{0.83}Co_{0.17}Al$-LDH are much different from pure $Ni_{0.83}Co_{0.17}Al$-LDH. It is found that $Ni_{0.83}Co_{0.17}Al$-LDH nanosheets with much smaller particle size than that of pure $Ni_{0.83}Co_{0.17}Al$-LDH grow uniformly on the surface of rGO. Close observation reveals that the LDH nanosheets arrays grow orderly on both sides of rGO sheets (Fig. 4D), which effectively prevents the rGO sheets from stacking and aggregation, giving rise to the construction of a sandwich structure. Such structure is also confirmed by the TEM image (Fig. 4E). It is found that the $Ni_{0.83}Co_{0.17}Al$-LDH nanosheets with about 10 nm thickness grow perpendicularly on the rGO substrate. Although the contrast between the rGO substrate and LDH nanosheets is not obvious, the graphene sheets are still found in the composite due to the well-known characteristic features. In the HRTEM image (Fig. 4F), the distance of the adjacent lattice fringes (marked by the arrows) is measured to be 0.26 nm, corresponding to the d_{012} value of rhombohedral NiAl-LDH. The corresponding FFT pattern (Fig. 4G) also shows the diffraction spots of the (012) planes for NiAl-LDH, revealing the single crystalline nature.

Generally, favorable specific surface area of the target electrode materials is expected for accommodating a large amount of superficial electrochemical active sites to participate in the Faradaic redox reactions.[33] The porosity and surface area of the composite are examined by N_2 adsorption/desorption. As shown in Fig. 5, a typical Langmuir type IV characteristic isotherm accompanied by an obvious hysteresis loop is observed

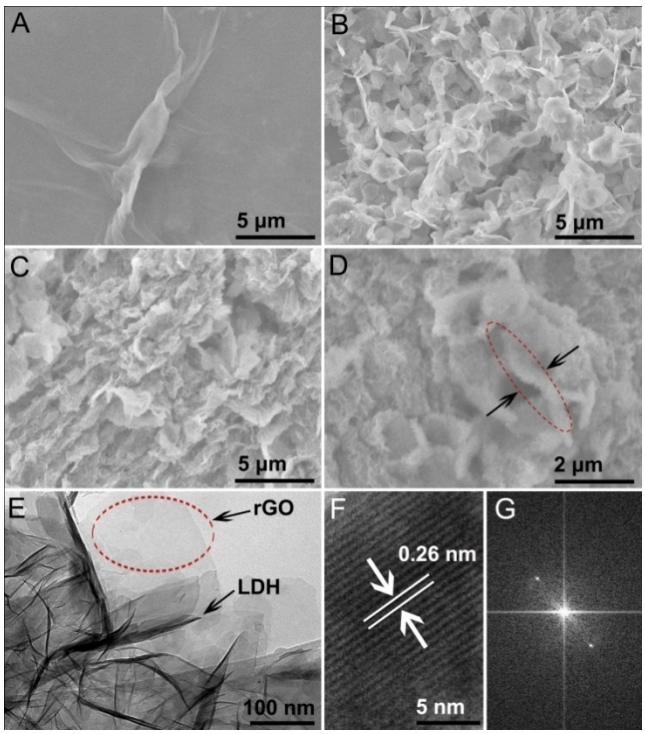

Fig. 4 SEM image of as-prepared (A) GO, (B) pure $Ni_{0.83}Co_{0.17}Al$-LDH; (C, D) SEM images with different magnification, (E) TEM image, (F) HRTEM image, and (G) the corresponding FTT pattern of rGO/$Ni_{0.83}Co_{0.17}Al$-LDH.

Table 1 Specific surface area, average pore diameter and total volume of RGL1, RGL2, RGL3, RGL4 and RGL5

Samples	S_{BET} (m^2/g)	D (nm)	V_P (cm^3/g)
RGL1	171.5	29.26	1.97
RGL2	137.6	28.24	0.89
RGL3	106.4	28.69	0.69
RGL4	98.0	23.49	0.51
RGL5	73.7	19.11	0.31

*S_{BET}, the BET specific surface area calculated in the relative pressures range from 0.05 to 0.2; D, the average diameter of mesopores calculated by the BJH method; V_p, the total pore volume calculated at the relative pressure of about 0.95.

Dalton Transactions Accepted Manuscript

This journal is © The Royal Society of Chemistry [year]

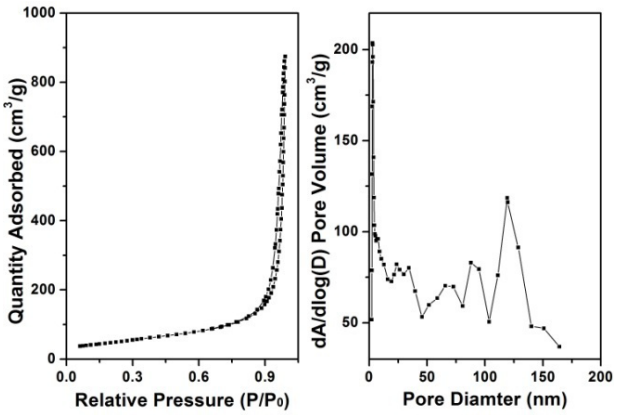

Fig. 5 N_2 adsorption/desorption isotherm (left) and the corresponding pore size distribution (right) of rGO/$Ni_{0.83}Co_{0.17}$Al-LDH.

in the curve of RGL1, suggesting the formation of mesopores.[54,55] The inset in the Fig. 5 shows the corresponding pore size distribution, which indicates a relatively wide pore size distribution. As summarized in Table 1, the BET surface area and the average pore size are calculated to be 171.5 m^2/g and 29.26 nm, respectively. And all the other hybrid composites with different Co doping show high BET surface area.The large surface area and suitable mesoporous pores of the hybrid composite are advantageous for the electrolyte ions to access the active materials, which may contribute to enhancement of capacitive performance.[56]

3.2. Electrochemical performance of rGO/$Ni_{1-x}Co_xAl$-LDH

To evaluate the electrochemical performance of as-prepared composites, cyclic voltammetry (CV) and galvanostatic charge-discharge measurements were performed. The CV curves of rGO/NiAl-LDH, rGO/CoAl-LDH and rGO/$Ni_{1-x}Co_x$Al-LDHs electrodes at the sweep rate of 2 mV s^{-1} are shown in Fig. 6. Strong redox peaks can be observed in the CV curves for all samples, indicating that the capacitive characteristics are mainly governed by Faradaic reaction. The peak couples can be attributed to the following Faradaic redox reactions of $Ni(OH)_2$ and $Co(OH)_2$.[42,43,57]

$$Ni(OH)_2 + OH^- \rightleftarrows NiOOH + H_2O + e^- \quad (1)$$

$$Co(OH)_2 + OH^- \rightleftarrows CoOOH + H_2O + e^- \quad (2)$$

$$CoOOH + OH^- \rightleftarrows CoO_2 + H_2O + e^- \quad (3)$$

It is found that the compositions of rGO/$Ni_{1-x}Co_x$Al-LDHs have an obvious influence on their redox peaks (Fig. 6B) compared with pure rGO/NiAl-LDH and rGO/CoAl-LDH (Fig. 6A). The potential difference (ΔE) between the oxidation potential and the reduction potential is generally taken as a measure of the reversibility of the electrode reaction.[46,58] It is found that the potential difference for all the composites is higher than the theoretical value of 59 mV for a reversible one-electron process, which means that the electrode process is quasi-reversible.[45] With the increase of Co content in rGO/$Ni_{1-x}Co_x$Al-LDHs, the potential difference decreases and is smaller than that of pure rGO/NiAl-LDH. Hence it is inferred that the reversibility for electrode reaction is greatly improved by doping of Co^{2+} ions. Because the specific capacitance is directly proportional to the area of the CV curve covered, RGL1 evidently has the highest specific capacitance among all the doped rGO/LDH composites.

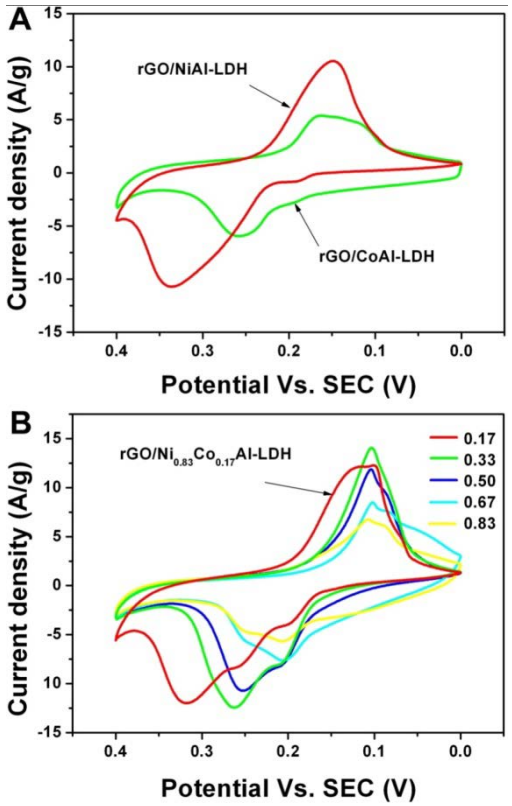

Fig. 6 The CV curves of (A) pure rGO/NiAl-LDH and rGO/CoAl-LDH, (B) rGO/$Ni_{1-x}Co_x$Al-LDH with different Co doping measured at a scan rate of 2 mV s^{-1} in the potential range of 0 – 0.4V.

Fig. 7 presents the galvanostatic charge and discharge curves of rGO/NiAl-LDH, rGO/CoAl-LDH and rGO/$Ni_{1-x}Co_x$Al-LDHs at the current density of 1 A/g in the potential range of 0–0.37 V. The redox characteristics in the charge-discharge curves are directly related with the redox peaks in the CV curves, corresponding to the redox reaction of nickel and cobalt hydroxides (Fig. 6). Obviously, the doping of cobalt has a significant effect on the charge/discharge curves profiles, due to the changes of the redox potential in the composites. The highest specific capacitance of RGL1 should be attributed to the unique structure and large specific surface, which are favourable for the proton diffusion during the charge and discharge processes. Fig. 8 gives the relationship between the specific capacitance of rGO/$Ni_{1-x}Co_x$Al-LDHs and Co doped content (x). In Table 2, the calculated specific capacitance is 1902, 1824, 1580, 1521 and 1404 F/g when the Co content is 0.17, 0.33, 0.50, 0.67 and 0.83, all of which are larger than 1132 F/g for pure rGO/CoAl-LDH. This may be caused by the gradual lost of sandwich structure (Fig. 3) and the decreased surface area (Table 1). Additionally, RGL1 has the larger specific capacitance than that of rGO/NiAl-LDH (1518 F/g). From our previous work,[48] rGO/NiAl-LDH has the similar structure and surface area to those of RGL1. Thus, the higher specific capacitance can be related with the enhanced conductivity by the doping of Co. Moreover, when the Co content is 0.83, the capacitance is lower than that of pure rGO/NiAl-LDH. As shown in Fig. 3, when the Co content is 0.83, the sandwich structure almost disappears and the specific surface area is markedly decreased (73.7 m^2/g), which is much lower than

Dalton Transactions Accepted Manuscript

that of

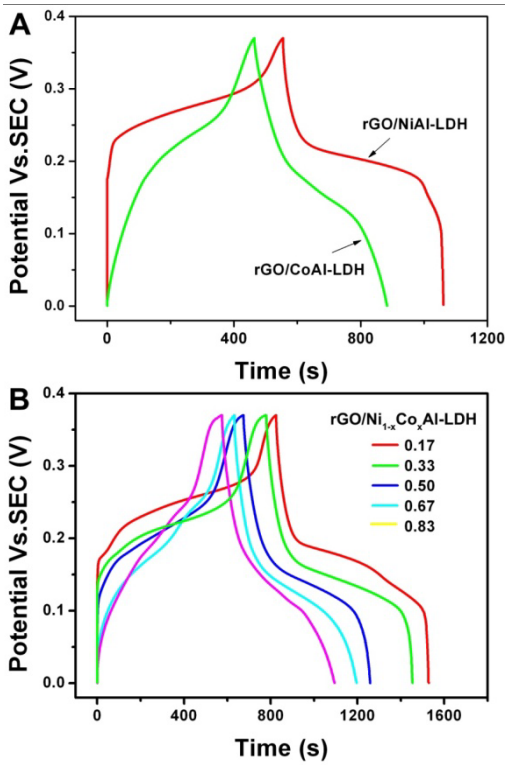

Fig. 7 The charge/discharge curves of (A) undoped rGO/NiAl-LDH and rGO/CoAl-LDH, (B) rGO/$Ni_{1-x}Co_xAl$-LDH at a current density of 1 A/g.

RGL1 (171.5 m^2/g), leading to slower mass and electron transfer for the faradic redox reactions, and further resulting in the low specific capacitance.[33,48] On basis of above analysis, we can infer that all the Co doping content, the structure and specific surface area play important roles in the specific capacitance of the final product. And the relationship is very sophisticated, which will be studied in detail by finely tuning the doped Co content in our future work.

The influence of discharge current density on the specific capacitance of rGO/$Ni_{1-x}Co_xAl$-LDH is shown in Fig. 9. The calculated specific capacitances at the different current densities are summarized in Table 2, meanwhile, the value of pure rGO/NiAl- LDH is also list for comparison. As shown in Table 2

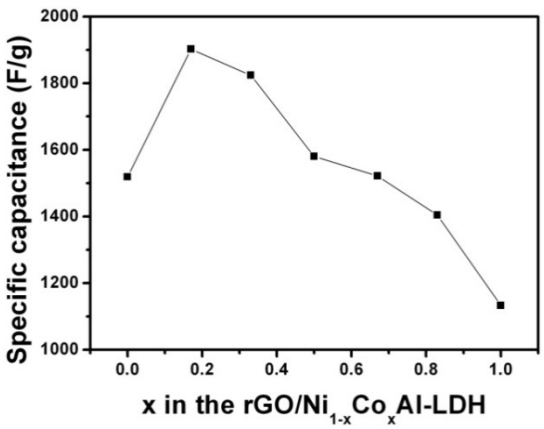

Fig. 8 Relationship between the specific capacitance and the doped Co content in rGO/$Ni_{1-x}Co_xAl$-LDH.

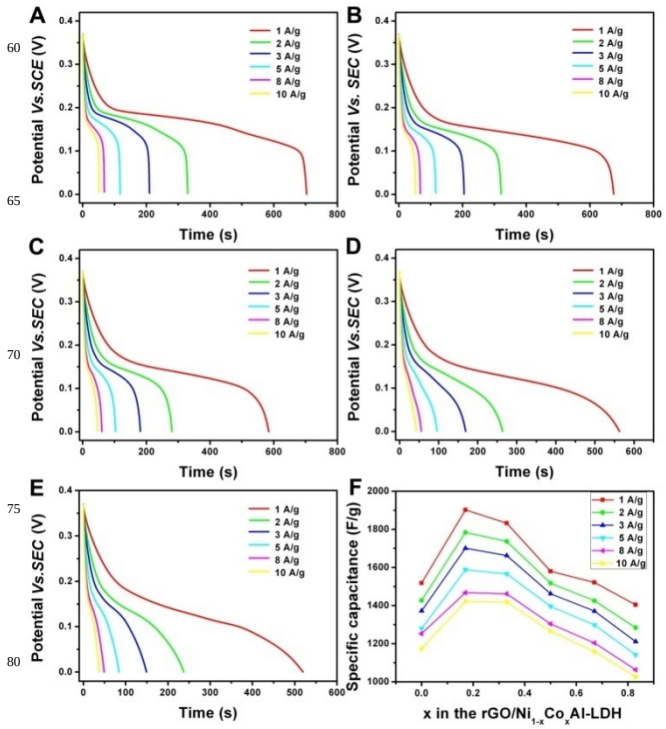

Fig. 9 The discharge curves of rGO/$Ni_{1-x}Co_xAl$-LDH with x values of (A) 0.17, (B) 0.33, (C) 0.50, (D) 0.67, (E) 0.83 measured at different current densities; (F) dependence of the specific capacitance on the different discharge current densities of rGO/$Ni_{1-x}Co_xAl$-LDH with different Co doping content.

Table 2 The specific capacitance of the rGO/$Ni_{1-x}Co_xAl$-LDH composites at different current densities

Csp (F/g) of composites	Current density (A/g)					
	1	2	3	5	8	10
rGO/NiAl	1518	1426	1372	1279	1253	1174
RGL1	1902	1784	1701	1588	1468	1422
RGL2	1832	1737	1662	1566	1462	1419
RGL3	1580	1517	1462	1396	1304	1266
RGL4	1521	1425	1371	1298	1204	1159
RGL5	1404	1284	1211	1142	1063	1027

and Fig. 9F, RGL1 exhibits excellent specific capacitances of 1902, 1784, 1701, 1588, 1468 and 1422 F/g at the different current densities of 1, 2, 3, 5, 8 and 10 A/g, respectively. The capacitance retention of RGL1 is still 75% when the discharge current density increases from 1 A/g to 10 A/g. In addition, the electrochemical performance of RGL2 and RGL3 is also better than that of un-doped rGO/NiAl-LDH without Co doping. The specific capacitance decreases rapidly when the Co content is further increased to 0.67 and 0.83, which may be attributed to the change of morphology and the decrease of the specific surface. It should be noted that the specific capacitance in our work are much better than that of NiCoAl-LDH-NWCNT, which has the specific capacitance of 1035 F/g at a current density of 1 A/g, and 57.7% of the capacitance retained as the current density increased to 10 A/g.

The cycling stability of electrode materials is an important requirement for their practical application. The cycling stability of RGL1 was examined by galvanostatic charge-discharge test for 1500 cycles at the current density of 10 A/g. Fig. 10 displays the specific capacitance and columbic efficiency (η) of RGL1 as a

Dalton Transactions Accepted Manuscript

This journal is © The Royal Society of Chemistry [year]

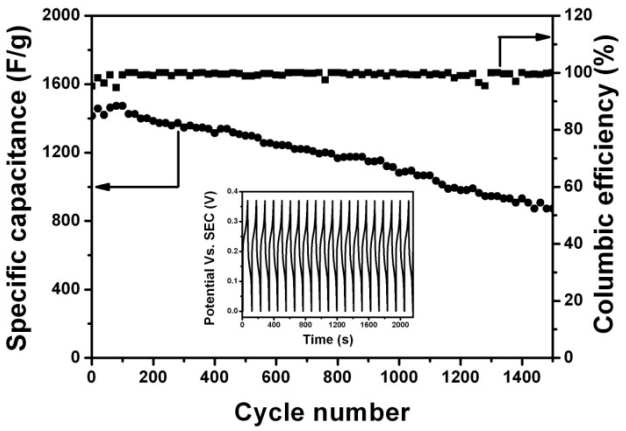

Fig. 10 The cycling performance and the corresponding columbic efficiency of rGO/$Ni_{0.83}Co_{0.17}$Al-LDH at the current density of 10 A/g. The inset is the first twenty charge/discharge curves.

function of the charge-discharge cycle numbers. The first twenty galvanostatic charge-discharge curves of the RGL1 electrodes are inserted in Fig. 10. The columbic efficiency of the capacitor can be calculated from the charge-discharge experiments as follows:

$$\eta\ (\%) = \Delta t_C/\Delta t_D \times 100 \quad (4)$$

where Δt_C and Δt_D are the charging and discharging times with the same current, respectively. The columbic efficiency is calculated to be 99%. It is found that the specific capacitance increases slightly over the first 100 cycles due to the complete activation of the active materials.[59] Then the capacitance of the composite gradually decreases at higher cycle numbers. After 1500cycles, 62% of the initial specific capacitance (from 1422 to 873 F/g) is remained at the high current density of 10 A/g, indicating the relatively high stability.

Electrochemical impedance spectroscopy (EIS) of rGO/$Ni_{1-x}Co_xAl$-LDHs was measured to further study the change of the reaction kinetics after the addition of Co^{2+}. Fig. 11 shows the Nyquist profiles of rGO/NiAl-LDH, RGL1, RGL2, RGL3, RGL4 and RGL5. All the impedance spectra of the composites include one depressed semicircle in the high frequency region and a sloped line in the low frequency region. It is well accepted that the semicircle reflects the electrochemical reaction impedance of the electrode relating to charge transfer through the electrode/

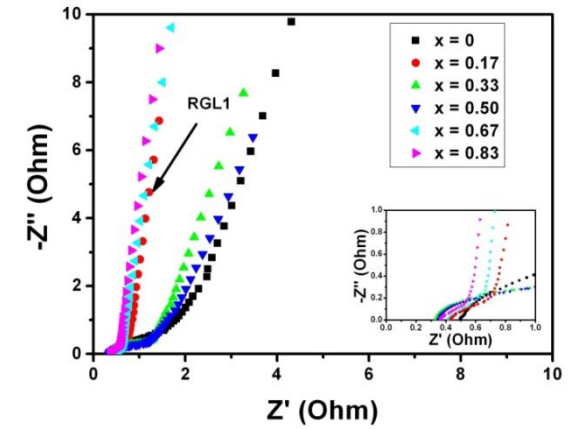

Fig. 11 Nyquist plots of rGO/NiAL-LDH, RGL1, RGL2, RGL3, RGL4 and RGL5 in 6 mol/L KOH. Insets are the impedances at high frequency region.

electrolyte interface, and the inclined line in the low-frequency region represents the Warburg impedance, which is related to diffusion of electroactive species.[54] Obviously, all the Co-doped rGO/$Ni_{1-x}Co_xAl$-LDH composites present a much smaller semicircle (enlarged view of high-frequency insert in Fig. 11 and a higher slope than that of pure LDH. This changing tendency is ascribed to the doping of Co, which increases the electronic conductivity and also acts as an electroactive material. The EIS results also show the RGL1 has a lower charge transfer resistance and ion diffusion resistance with fast reaction kinetics.

4. Conclusion

In summary, a series of rGO/$Ni_{1-x}Co_xAl$-LDH hybrid composites with different Co doping content have been successfully fabricated by employing AlOOH as aluminum source, followed by an *in situ* growth process. Among the different ratios of cobalt to nickel, rGO/$Ni_{0.83}Co_{0.17}$Al-LDH exhibits interesting sandwich structure, offers highest capacitance and good cycling stability, which are due to the enhanced conductivity by the doping of cobalt, large specific surface area, mesopore structure and large pore volume. This composite prepared through a facile synthetic route may hold great promise as electrode materials for high-performance supercapacitors. In particular, the *in situ* synthesis procedure may pave a way to prepare other LDH/graphene composites with interesting structures, which are potential in supercapacitors and other fields.

Acknowledgements

Financial supports from the National Natural Science Foundation of China (NSFC 21271053, 21001035, 51272050, 51072038), Research Fund for the Doctoral Program of Higher Education of China (20112304110021), Natural Science Foundation of Heilongjiang Province (LC2012C10), Program for New Century Excellent Talents in University, Harbin Sci.-Tech. Innovation Foundation (RC2012XK017012), and the Fundamental Research Funds for the Central Universities of China are greatly acknowledged.

Notes and references

[a] *Key Laboratory of Superlight Materials and Surface Technology, Ministry of Education, College of Material Sciences and Chemical Engineering, Harbin Engineering University, Harbin 150001, PR China; E-mail: yangpiaoping@hrbeu.edu.cn; gaopeng@hrbeu.edu.cn*

[b] *College of Sciences, Harbin Engineering University, Harbin 150001, P. R. China; Chenyujin@hrbeu.edu.cn*

† Electronic Supplementary Information (ESI) available: EDS analysis, XRD patterns of rGO/$Ni_{1-x}Co_xAl$-LDH with different cobalt compositiion, XPS of RGL1, SEM image of rGO/CoAl-LDH. See DOI:10.1039/b000000x/

1 M. Winter and R.J. Brodd, *Chem. Rev.* 2004, **104**, 4245.
2 M.D. Stoller, S. Park, Y. Zhu, J. An and R.S. Ruoff, *Nano Lett.* 2008, **8**, 3498.
3 L. L. Zhang and X. S. Zhao, *Chem. Soc. Rev.* 2009, **38**, 2520.
4 J.R. Miller and P. Simon, *Science* 2008, **321**, 651.
5 X. Huang, X. Qi, F. Boey and H. Zhang, *Chem. Soc. Rev*. 2012, **41**, 666.
6 Z. Fan, J. Yan, L. Zhi, Q. Zhang, T. Wei, J. Feng, M. Zhang, W. Qian and F. Wei, *Adv. Mater.* 2010, **22**, 3723.
7 L. Zhao, L.-Z. Fan, M.-Q. Zhou, H. Guan, S. Qiao, M. Antonietti and M.-M. Titirici, *Adv. Mater.* 2010, **22**, 5202.

Dalton Transactions Accepted Manuscript

8 J. Yang, C. Yu, X. Fan, Z. Ling, J. Qiu and Y. Gogotsi, *J. Mater. Chem. A* 2013, **1**, 1963.
9 J. Zhang, J. Jiang, H. Li and X. S. Zhao, *Energy Environ. Sci.* 2011, **4**, 4009.
10 L. L. Zhang, X. Zhao, M. D. Stoller, Y. Zhu, H. Ji, S. Murali, Y. Wu, S. Perales, B. Clevenger and R. S. Ruoff, *Nano Lett.* 2012, **12**, 1806.
11 C. Liu, F. Li, L.-P. Ma and H.-M. Cheng, *Adv. Mater*. 2010, **22**, E28.
12 K. Zhang, L.L. Zhang and X. S. Zhao, J. Wu, *Chem. Mater*. 2010, **22**, 1392.
13 Q. Wu, Y. Xu, Z. Yao, A. Liu and G. Shi, *ACS Nano* 2010, **4**, 1963.
14 L.J. Cote, R. Cruz-Silva and J. Huang, *J. Am. Chem. Soc*. 2009, **131**, 11027.
15 C.-C. Hu, K.-H. Chang, M.-C. Lin and Y.-T. Wu, *Nano Lett*. 2006, **6**, 2690.
16 C. Xu, X. Wang, J. Zhu, X. Yang and L. Lu, *J. Mater. Chem*. 2008, **18**, 5625.
17 X. Zhang, W. Shi, J. Zhu, W. Zhao, J. Ma, S. Mhaisalkar, T. Maria, Y. Yang, H. Zhang, H. Hng and Q. Yan, *Nano Res*. 2010, **3**, 643.
18 S. Chen, J. Zhu, X. Wu, Q. Han, X. Wang, *ACS Nano* 2010, 2822.
19 J. Ji, L. L. Zhang, H. Ji, Y. Li, X. Zhao, X. Bai, X. Fan, F. Zhang and R. S. Ruoff, *ACS Nano* 2013, **7**, 6237.
20 Z.-S. Wu, W. Ren, D.-W. Wang, F. Li, B. Liu and H.-M. Cheng, *ACS Nano* 2010, **4**, 5835.
21 L. L. Zhang, Z. Xiong and X. S. Zhao, *J. Power Sources* 2013, **222**, 326.
22 J. Wang, Y. Song, Z. Li, Q. Liu, J. Zhou, X. Jing, M. Zhang and Z. Jiang, *Energy Fuels* 2010, **24**, 6463.
23 Z.-S. Wu, D.-W. Wang, W. Ren, J. Zhao, G. Zhou, F. Li and H.-M. Cheng, *Adv. Funct. Mater.* 2010, **20**, 3595.
24 Y. Niu, R. Li, Z. Li, Y. Fang and J. Liu, *Electrochim. Acta* 2013, **94**, 360.
25 S. Huang, G.-N. Zhu, C. Zhang, W.W. Tjiu, Y.-Y. Xia and T. Liu, *ACS Appl. Mater. Interfaces* 2012, **4**, 2242.
26 L. Zhang, J. Wang, J. Zhu, X. Zhang, K. San Hui and K.N. Hui, *J. Mater. Chem. A* 2013, **1**, 9046.
27 Q. Wang, D and O'Hare, *Chem. Rev*. 2012, 112, 4124.
28 S. He, Z. An, M. Wei, D.G. Evans and X. Duan, *Chem. Commun*. 2013, **49**, 5912.
29 Y. Zhao, B. Li, Q. Wang, W. Gao, C. J. Wang, M. Wei, D. G. Evans, X. Duan and D. O'Hare, *Chem. Sci.* 2014, **5**, 951.
30 Z. Liu, R. Ma, M. Osada, N. Iyi, Y. Ebina, K. Takada and T. Sasaki, *J. Am. Chem. Soc*. 2006, **128**, 4872.
31 J.L. Gunjakar, I.Y. Kim, J.M. Lee, N.-S. Lee and S.-J. Hwang, *Energy Environ. Sci*. 2013, **6**, 1008.
32 S. Yang, X. Feng, X. Wang and K. Müllen, *Angew. Chem. Int. Ed*. 2011, **50**, 5339.
33 M. Shao, F. Ning, Y. Zhao, J. Zhao, M. Wei, D.G. Evans and X. Duan, *Chem. Mater*. 2012, **24**, 1192.
34 Y. Guo, Z. Zhu, Y. Qiu and J. Zhao, *Chem. Eng. J*. 2013, **219**, 69.
35 A. Garcia-Gallastegui, D. Iruretagoyena, V. Gouvea, M. Mokhtar, A.M. Asiri, S.N. Basahel, S.A. Al-Thabaiti, A.O. Alyoubi, D. Chadwick and M.S.P. Shaffer, *Chem. Mater*. 2012, **24**, 4531.
36 J.-M. Oh, D.-H. Park, S.-J. Choi and J.-H. Choy, *Recent Pat. Nanotechnol*. 2012, **6**, 200.
37 C. Chen, L.K. Yee, H. Gong, Y. Zhang and R. Xu, *Nanoscale* 2013, **5**, 4314.
38 D. Pan and H. Zhang, *Acta Chim. Sin*. 2011, **69**, 1545.
39 Y. Wang, D. Zhang, Q. Bao, J. Wu and Y. Wan, *J. Mater. Chem*. 2012, **22**, 23106.
40 X.-M. Liu, Y.-H. Zhang, X.-G. Zhang and S.-Y. Fu, *Electrochim. Acta* 2004, **49**, 3137.
41 Z. Lu, W. Zhu, X. Lei, G.R. Williams, D. O'Hare, Z. Chang, X. Sun and X. Duan, *Nanoscale* 2012, **4**, 3640.
42 V. Gupta, S. Gupta and N. Miura, *J. Power Sources* 2009, **189**, 1292.
43 C. Yu, J. Yang, C. Zhao, X. Fan, G. Wang and J. Qiu, *Nanoscale*, 2014, **6**, 3097.
44 M. Li, J.E. Zhu, L. Zhang, X. Chen, H. Zhang, F. Zhang, S. Xu and D.G. Evans, *Nanoscale* 2011, **3**, 4240.
45 Z.-A. Hu, Y.-L. Xie, Y.-X. Wang, H.-Y. Wu, Y.-Y. Yang and Z.-Y. Zhang, *Electrochim. Acta* 2009, **54**, 2737.
46 X. Liu, J. Huang, X. Wei, C. Yuan, T. Liu, D. Cao, J. Yin and G. Wang, *J. Power Sources* 2013, **240**, 338.
47 Y. Zhao, S. He, M. Wei, D.G. Evans and X. Duan, *Chem. Commun*. 2010, **46**, 3031.
48 J. Xu, S. Gai, F. He, N. Niu, P. Gao, Y. Chen and P. Yang, *J. Mater. Chem*. A 2014, **2**, 1022.
49 C. Xu, X. Wang and J. Zhu, *J. Phys. Chem. C* 2008, **112**, 19841.
50 H.-J. Shin, K.K. Kim, A. Benayad, S.-M. Yoon, H.K. Park, I.-S. Jung, M.H. Jin, H.-K. Jeong, J.M. Kim, J.-Y. Choi and.H. Lee, *Adv. Funct. Mater*. 2009, **19**, 1987.
51 J. Fang, M. Li, Q. Li, W. Zhang, Q. Shou, F. Liu, X. Zhang and J. Cheng, *Electrochim. Acta* 2012, **85**, 248.
52 S.Y. Han, I.Y. Kim, K.Y. Jo and S.-J. Hwang, *J. Phys. Chem. C* 2012, **116**, 7269.
53 Z. Gao, J. Wang, Z. Li, W. Yang, B. Wang, M. Hou, Y. He, Q. Liu, T. Mann, P. Yang, M. Zhang and L. Liu, *Chem. Mater.* 2011, **23**, 3509.
54 J. Li, S. Xiong, Y. Liu, Z. Ju and Y. Qian, *ACS Appl. Mater. Interfaces* 2013, **5**, 981.
55 D.N. Futaba, K. Hata, T. Yamada, T. Hiraoka, Y. Hayamizu, Y. Kakudate, O. Tanaike, H. Hatori, M. Yumura and S. Iijima, *Nat. Mater*. 2006, **5**, 987.
56 S.B. Kulkarni, A.D. Jagadale, V.S. Kumbhar, R.N. Bulakhe, S.S. Joshi and C.D. Lokhande, *Int. J. Hydrogen Energy* 2013, **38**, 4046.
57 F. Zhang, J. Jiang, C. Yuan, L. Hao, L. Shen, L. Zhang and X. Zhang, *J. Solid State Electrochem*. 2012, **16**, 1933.
58 L. Xie, Z. Hu, C. Lv, G. Sun, J. Wang, Y. Li, H. He, J. Wang and K. Li, *Electrochim. Acta* 2012, **78**, 205.
59 M.-C. Liu, L.-B. Kong, C. Lu, X.-M. Li, Y.-C. Luo and L. Kang, *ACS Appl. Mater. Interfaces* 2012, **4**, 4631.

Dalton Transactions Accepted Manuscript

This journal is © The Royal Society of Chemistry [year]

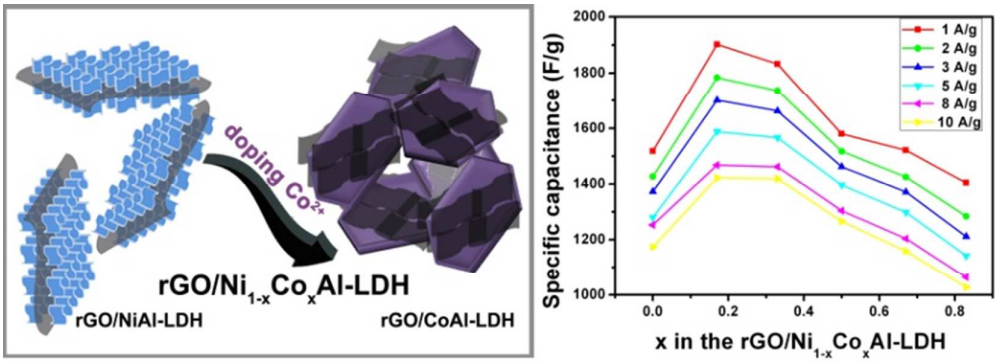

A novel sandwich-structured rGO/$Ni_{0.83}Co_{0.17}$Al-LDH hybrid composite exhibits high supercapacitor performance: the specific capacitance of 1902 F/g at 1 A/g and excellent cycling stability.

Dalton Transactions Accepted Manuscript